Inorganic Chemistry

Article

pubs.acs.org/IC

Unraveling the Electronic Structures of Low-Valent Naphthalene and Anthracene Iron Complexes: X-ray, Spectroscopic, and Density Functional Theory Studies

Eva-Maria Schnöckelborg,[†] Marat M. Khusniyarov,[§] Bas de Bruin,[⊥] František Hartl,[∥] Thorsten Langer,[†] Matthias Eul,[†] Stephen Schulz,[†] Rainer Pöttgen,[†] and Robert Wolf*[,†,‡]

[†]Institute of Inorganic and Analytical Chemistry, University of Münster, Corrensstrasse 30, 48149 Münster, Germany

[‡]Institute of Inorganic Chemistry, University of Regensburg, 93040 Regensburg, Germany

[§]Department of Chemistry and Pharmacy, Friedrich-Alexander-Universität Erlangen-Nürnberg, Egerlandstraße 1, 91058 Erlangen, Germany

[⊥]Homogeneous and Supramolecular Catalysis, Van't Hoff Institute for Molecular Sciences, University of Amsterdam, Science Park 904, 1098 XH Amsterdam, The Netherlands

[∥]Department of Chemistry, University of Reading, Whiteknights, Reading, RG6 6AD, United Kingdom

Supporting Information

ABSTRACT: Naphthalene and anthracene transition metalates are potent reagents, but their electronic structures have remained poorly explored. A study of four Cp*-substituted iron complexes (Cp* = pentamethylcyclopentadienyl) now gives rare insight into the bonding features of such species. The highly oxygen- and water-sensitive compounds [K(18-crown-6){Cp*Fe(η^4-$C_{10}H_8$)}] (**K1**), [K(18-crown-6){Cp*Fe(η^4-$C_{14}H_{10}$)}] (**K2**), [Cp*Fe(η^4-$C_{10}H_8$)] (**1**), and [Cp*Fe(η^4-$C_{14}H_{10}$)] (**2**) were synthesized and characterized by NMR, UV−vis, and ^{57}Fe Mössbauer spectroscopy. The paramagnetic complexes **1** and **2** were additionally characterized by electron paramagnetic resonance (EPR) spectroscopy and magnetic susceptibility measurements. The molecular structures of complexes **K1**, **K2**, and **2** were determined by single-crystal X-ray crystallography. Cyclic voltammetry of **1** and **2** and spectroelectrochemical experiments revealed the redox properties of these complexes, which are reversibly reduced to the monoanions [Cp*Fe(η^4-$C_{10}H_8$)]$^-$ (**1**$^-$) and [Cp*Fe(η^4-$C_{14}H_{10}$)]$^-$ (**2**$^-$) and reversibly oxidized to the cations [Cp*Fe(η^6-$C_{10}H_8$)]$^+$ (**1**$^+$) and [Cp*Fe(η^6-$C_{14}H_{10}$)]$^+$ (**2**$^+$). Reduced orbital charges and spin densities of the naphthalene complexes **1**$^{-/0/+}$ and the anthracene derivatives **2**$^{-/0/+}$ were obtained by density functional theory (DFT) methods. Analysis of these data suggests that the electronic structures of the anions **1**$^-$ and **2**$^-$ are best represented by low-spin Fe^{II} ions coordinated by anionic Cp* and dianionic naphthalene and anthracene ligands. The electronic structures of the neutral complexes **1** and **2** may be described by a superposition of two resonance configurations which, on the one hand, involve a low-spin Fe^{I} ion coordinated by the neutral naphthalene or anthracene ligand L, and, on the other hand, a low-spin Fe^{II} ion coordinated to a ligand radical L$^{\bullet-}$. Our study thus reveals the redox noninnocent character of the naphthalene and anthracene ligands, which effectively stabilize the iron atoms in a low *formal*, but significantly higher *spectroscopic* oxidation state.

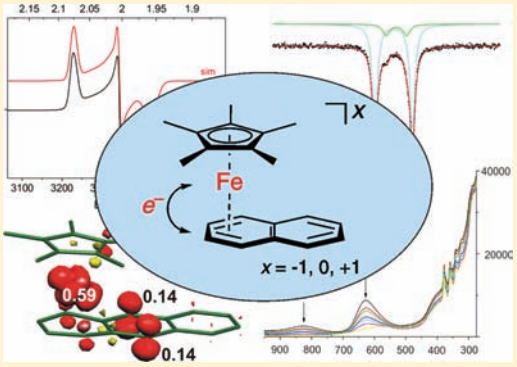

INTRODUCTION

Anionic naphthalene and anthracene transition metal complexes are exciting "transition metal anion reagents" that are increasingly attracting attention in synthetic and catalytic applications.[1,2] Homoleptic metalates have been reported for a number of transition metals. Typical representatives are complexes **A** and **B**, that contain the electron-poor metals Ti, Zr, Hf, Nb, and Ta. Complexes of more electron-rich transition metals such as the bis(anthracene)ferrate anion **C** are still rather scarce.[3−6] Moreover, heteroleptic metalates are also very uncommon, and the Cp*-substituted titanium complex **D** is one of only a few examples.[6b,7]

The molecular structures of the polyarene metalates **A**−**D** feature η^4-coordinated naphthalene or anthracene molecules. The polyarene ligands can be readily substituted to produce reduced carbonyl, alkene, and isocyanide complexes.[2,3,5−9] Furthermore, it is noteworthy that the reaction of the complex [Ti(η^4-$C_{10}H_8$)$_3$]$^{2-}$ (**A**, M = Ti) and P_4 yielded the highly unusual decaphosphatitanocene sandwich [Ti(η^4-P_5)$_2$]$^{2-}$.[10] We recently examined reactions of complex [Fe(η^4-$C_{14}H_{10}$)$_2$]$^-$ (**C**) and the related cobaltate anion [Co(η^4-$C_{14}H_{10}$)$_2$]$^-$. Both

Received: February 17, 2012
Published: May 25, 2012

complexes react with phosphaalkynes RC≡P to give unprecedented diphosphacyclobutadiene sandwich anions $[M(\eta^4\text{-}P_2C_2R_2)_2]^-$.[11] In contrast, an unusual hexaphenylbenzene complex is formed in the reaction of **C** with diphenylacetylene via alkyne cyclotrimerization.[12] Very recently, we showed that complex **C** is a competent precatalyst in iron-catalyzed cross-coupling reactions, which shows that polyarene metalate anions may also find use in catalytic applications.[13]

Chart 1

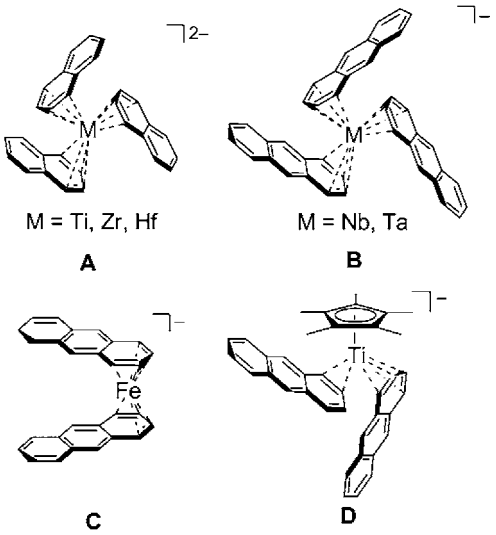

The examples mentioned above demonstrate the high synthetic utility of naphthalene and anthracene metalates. The synthetic potential of these reagents is increasingly being realized in different synthetic applications. To expand polyarene metalate chemistry further it is necessary to develop a more diverse array of metalates, in particular new heteroleptic derivatives. Furthermore, an improved understanding of the bonding situation in the polyarene metalates is required.

To our knowledge, no detailed investigations of the bonding situation of complexes **A**–**D** or related naphthalene and anthracene metalates have been reported to date. Moreover, there are only very few studies concerning related, neutral transition metal polyarene complexes in the literature.[14,15] A detailed investigation of the electronic structures and the spectroscopic characteristics of suitable polyarene transition metal complexes therefore seems timely to us and should provide valuable new insight. Here, we describe a case study of four closely related naphthalene and anthracene iron complexes that were recently prepared in our laboratory. We report the syntheses and the molecular structures of the Cp*-substituted compounds $[K(18\text{-crown-6})\{Cp^*Fe(\eta^4\text{-}C_{10}H_8)\}]$ (**K1**), $[K(18\text{-crown-6})\{Cp^*Fe(\eta^4\text{-}C_{14}H_{10})\}]$ (**K2**), $[Cp^*Fe(\eta^4\text{-}C_{10}H_8)]$ (**1**), and $[Cp^*Fe(\eta^4\text{-}C_{14}H_{10})]$ (**2**).[16] These compounds are rare examples of stable, crystalline polyarene iron complexes with the metal in the formal oxidation states 0 and +I.[17] The spectroscopic, magnetic, and redox properties of the complexes are described (NMR, EPR, ^{57}Fe Mössbauer, and UV–vis spectroscopy, cyclic voltammetry, and UV–vis spectroelectrochemistry). Density functional theory (DFT) calculations are used to analyze the spectroscopic results and to gain insight into the electronic structures of these unusual compounds.

RESULTS

Synthesis of Naphthalene and Anthracene Iron Complexes K1, K2, 1, and 2. In pursuit of new Cp*-substituted polyarene iron complexes, we studied the reduction of "Cp*FeCl" with potassium naphthalenide and potassium anthracenide. Cp*FeCl decomposes rapidly into Cp^*_2Fe and $FeCl_2$ at room temperature in solution, but cooled solutions are relatively stable.[18] Therefore, we developed a one-pot procedure where a solution of Cp*Li and $FeCl_2(thf)_{1.5}$ is first prepared in DME. This solution is then added at low temperature to solutions of potassium naphthalenide or potassium anthracenide to form the target compounds. Dark brown $[K(18\text{-crown-6})\{Cp^*Fe(\eta^4\text{-}C_{10}H_8)\}]$ (**K1**) can be isolated in up to 50% yield using this approach (Scheme 1a).

Scheme 1. Preparation of Low-Valent Naphthalene and Anthracene Complexes K1, K2, and 2 by the Reduction of "Cp*FeCl" with Potassium Naphthalenide or Potassium Anthracenide[a]

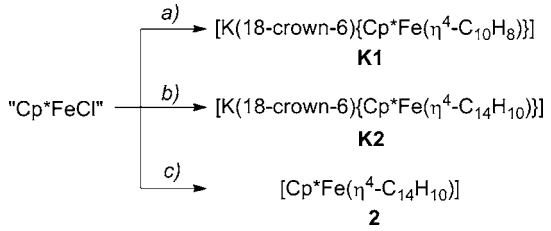

[a]Reagents: (*a*) 2 equiv of $KC_{10}H_8$, 18-crown-6; (*b*) 2 equiv of $KC_{14}H_{10}$, 18-crown-6; (*c*) 2 equiv of $KC_{14}H_{10}$, 18-crown-6 *not* added.

The dark green anthracene complex $[K(18\text{-crown-6})\{Cp^*Fe(\eta^4\text{-}C_{14}H_{10})\}]$ (**K2**) was obtained analogously from the reaction of $Cp^*Li/FeCl_2(thf)_{1.5}$ with 2 equiv of potassium anthracenide (Scheme 1b). However, it is difficult to isolate compound **K2** in high purity via this route because the samples typically contain free anthracene, which is difficult to remove because of its similar solubility. For this reason, we developed a more convenient synthesis of **K2** via a ligand exchange protocol (Scheme 2a). Stirring a tetrahydrofuran (THF) solution of

Scheme 2. Preparation of Complexes 1 and K2[a]

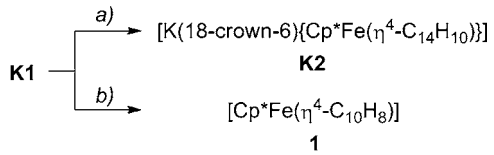

[a]Reagents (*a*) excess anthracene, (*b*) AgOTf.

naphthalene complex **K1** with anthracene for several days gives a forest green solution from which **K2** can be isolated as dark green crystals in modest, though reproducible yield (16%) and good purity. The neutral anthracene complex $[Cp^*Fe(\eta^4\text{-}C_{14}H_{10})]$ (**2**) is obtained from the reaction of potassium anthracenide and $Cp^*Li/FeCl_2(thf)_{1.5}$ (2:1) when the addition of crown ether to the reaction solution is omitted (Scheme 1c). Compound **2** dissolves well in nonpolar solvents and can thus be isolated in 24% yield by extracting the raw product of the reaction with *n*-hexane.[19] In contrast, we did not observe the neutral naphthalene complex $[Cp^*Fe(\eta^4\text{-}C_{10}H_8)]$ (**1**) in the 2:1 reaction of potassium naphthalenide with "Cp*FeCl".

dx.doi.org/10.1021/ic300366m | Inorg. Chem. 2012, 51, 6719–6730

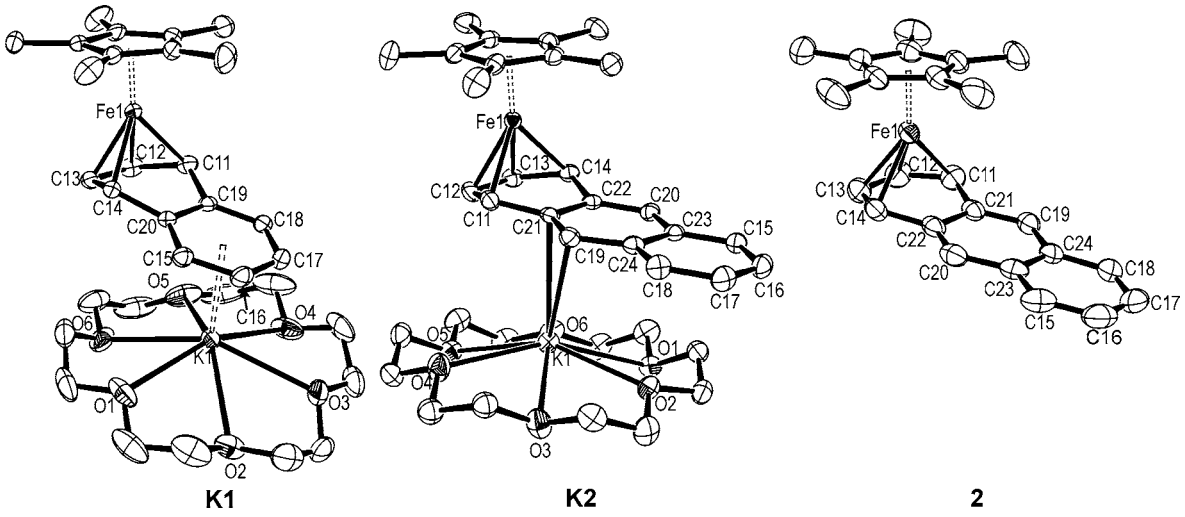

Figure 1. Single-crystal X-ray structures of complexes **K1**, **K2**, and **2**. Displacement ellipsoids are drawn at the 40% level; hydrogen atoms have been omitted for clarity; only one of the two crystallographically independent molecules of **K2** is shown.

Instead, this complex can be prepared by oxidizing **K1** with 1 equiv of AgOTf (Scheme 2b). Dark blue **1** was isolated in up to 47% yield by crystallization from *n*-hexane.

Molecular Structures. The molecular structures of the complexes [K(18-crown-6){Cp*Fe(η^4-$C_{10}H_8$)}] (**K1**), [K(18-crown-6){Cp*Fe(η^4-$C_{14}H_{10}$)}] (**K2**), and [Cp*Fe(η^4-$C_{14}H_{10}$)] (**2**) were determined by X-ray crystallography (Figure 1 and Table 1). The structure of **K1** shows an ion-contact pair of the

Table 1. Selected Structural Data of Complexes K1, K2, and 2

	K1	K2[a]	2
C11–C12	1.443(3)	1.431(2)	1.414(3)
C12–C13	1.405(3)	1.409(2)	1.388(4)
C13–C14	1.447(3)	1.429(2)	1.411(3)
Fe1–C11	2.076(2)	2.0806(15)	2.079(2)
Fe1–C12	1.980(2)	1.9997(15)	2.022(2)
Fe1–C13	1.975(2)	1.9894(17)	2.023(2)
Fe1–C14	2.0700(19)	2.0791(17)	2.061(2)
Fe1–C19	2.8287(19)		
Fe1–C20	2.8128(19)		
Fe1–C21		2.6027(19)	2.4561(17)
Fe1–C22		2.6363(18)	2.4279(16)
av. Fe1–C(Cp*)	2.048	2.059	2.0789
fold angle	35.1[b]	21.8[c]	15.8[c]

[a]One of two crystallographically independent molecules in the asymmetric unit. [b]Dihedral angle C11,C12,C13,C14/C11,C19,C20,C14. [c]Dihedral angle C11,C12,C13,C14/C11,C21,C22,C14.

[Cp*Fe(η^4-$C_{10}H_8$)}]$^-$ anion ($\mathbf{1}^-$) and the [K(18-crown-6)]$^+$ cation. In the anion, the Cp* moiety is η^5-coordinated to the iron (Fe1–C1,C2,C3,C4,C5 2.029(2)–2.073(2) Å) and the naphthalene ligand is η^4-coordinated (Fe1–C11,C12,C13,C14 1.975(2)–2.076(2) Å; Fe1–C19,C20 >2.8 Å). The coordinated arene ring of the naphthalene ligand is folded by 35.1° about the C11–C14 axis. The potassium cation is surrounded by one molecule 18-crown-6 and the naphthalene ligand, which coordinates to potassium in an η^6-fashion via the second arene ring [K1–C15,C16,C17,C18,C19,C20 3.152(2)–3.477(2) Å, Table 1].

Anthracene complex **K2** (Figure 1) displays two crystallographically independent molecules in the asymmetric unit which have very similar structures; hence, only one of them is discussed here. The structure of **K2** is closely related to **K1**, but a smaller fold angle (21.8°) of the arene ring coordinated to iron is observed. Furthermore, the coordination of the potassium cation by the anthracene ligand is more aptly described as an η^2-interaction in this case (K1–C19 3.543(14) Å, K1–C21 3.111(14) Å). The structure of neutral complex **2** (Figure 1) also shows an η^4-coordinated anthracene ligand (Fe1–C11,C12,C13,C14 2.022–2.079 Å), which displays an even smaller fold angle (15.8°) of the coordinated arene ring.

Unfortunately, repeated attempts to determine the molecular structure of complex [Cp*Fe(η^4-$C_{10}H_8$)] (**1**) failed because of the insufficient quality of the extremely thin, needle-like crystals. To be able to compare the structures of anionic, neutral, and cationic derivatives $\mathbf{1}^-/\mathbf{1}/\mathbf{1}^+$ and $\mathbf{2}^-/\mathbf{2}/\mathbf{2}^+$, we therefore optimized the geometries of these complexes with DFT methods at the BP86/def2-TZVP level.[20−23] For comparison, we also optimized the structures of the cations [Cp*Fe(η^6-$C_{10}H_8$)]$^+$ ($\mathbf{1}^+$) and [Cp*Fe(η^6-$C_{14}H_{10}$)]$^+$ ($\mathbf{2}^+$). Key structural parameters are summarized in Table 2. The DFT-

Table 2. Key Structural Parameters of the DFT-Optimized Structures of Complexes $\mathbf{1}^-$, 1, $\mathbf{1}^+$, $\mathbf{2}^-$, 2, and $\mathbf{2}^+$[a]

	$\mathbf{1}^-$	1	$\mathbf{1}^+$	$\mathbf{2}^-$	2	$\mathbf{2}^+$
Fe1–C19	2.900	2.543	2.202			
Fe1–C20	2.901	2.542	2.202			
Fe1–C21				2.818	2.318	2.237
Fe1–C22				2.816	2.323	2.237
fold angle	38.2[b]	20.0[b]	5.2[b]	31.6[c]	10.3[c]	7.1[c]

[a]The same numbering scheme is used as for the single-crystal X-ray structures. [b]Dihedral angle C11,C12,C13,C14/C11,C19,C20,C14. [c]Dihedral angle C11,C12,C13,C14/C11,C21,C22,C14.

optimized structures of [Cp*Fe(η^4-$C_{10}H_8$)]$^-$ ($\mathbf{1}^-$), [Cp*Fe(η^4-$C_{14}H_{10}$)]$^-$ ($\mathbf{2}^-$), and [Cp*Fe(η^4-$C_{14}H_{10}$)] (**2**) agree very well with the crystallographically determined ones (Tables 1 and 2). In the anions $\mathbf{1}^-$ and $\mathbf{2}^-$, the η^4-coordinated naphthalene and anthracene ligands show large fold angles of the aromatic ring ($\mathbf{1}^-$: 38.2°, $\mathbf{2}^-$: 31.6°). The aromatic rings are significantly less

dx.doi.org/10.1021/ic300366m | *Inorg. Chem.* 2012, 51, 6719–6730

folded in the neutral complexes **1** and **2**, which display fold angles for the coordinated polyarene ring of 20.0° (**1**) and 10.3° (**2**). The cations $\mathbf{1}^+$ and $\mathbf{2}^+$ clearly display nearly planar η^6-coordinated polyarene ligands.

NMR Spectra of Complexes K1, K2, 1, and 2. At room temperature, the ^{1}H NMR spectra of the diamagnetic compounds [K(18-crown-6){Cp*Fe(η^4-$C_{10}H_8$)}] (**K1**) and [K(18-crown-6){Cp*Fe(η^4-$C_{14}H_{10}$)}] (**K2**) exhibit severe line broadening, which is probably due to a fluxional process. Reasonably resolved spectra were obtained at low temperatures, however, which support the compositions shown by the single-crystal X-ray structures (Supporting Information, Figures S1 and S2).[24] The ^{1}H NMR spectrum of **K1** in THF-d_8 at −40 °C shows four resonances of the coordinated naphthalene ligand at 0.42, 4.80, 5.21, and 5.30 ppm. A broad singlet is observed for the Cp* ligand in the usual range at 1.71 ppm. The high-field resonance at 0.42 ppm may be assigned to the 1,4-protons. Such a high-field shift is typical for naphthalene ligands coordinated in an η^4-fashion to a low-valent transition metal center.[6] The ^{1}H NMR spectrum of **K2** in toluene-d_8 at −80 °C is similar to **K1** and displays signals of the coordinated anthracene ligand at 1.6, 4.6, 5.3, 6.2, and 6.5 ppm. A broad singlet at 2.3 ppm is assigned to the Cp* ligand.

The ^{13}C{^{1}H} NMR spectra of **K1** and **K2** also support their formulation as η^4-naphthalene and η^4-anthracene complexes, respectively. The signals for the carbon atoms coordinated to iron (44.9 and 72.4 ppm for **K1**, 51.2 and 72.9 ppm for **K2**) are shifted upfield compared to the free ligands. As observed in other η^4-coordinated complexes, the signals of the quarternary carbon atoms of the naphthalene ligand in **K1** (157.0 ppm) are shifted to lower field compared to the free naphthalene molecule.[25] The quarternary carbon signals of anthracene in complex **K2** (137.1 and 144.1 ppm) are in a similar range as in free anthracene.

Complexes **1** and **2** are paramagnetic, and their ^{1}H NMR spectra therefore suffer from severe line broadening. A very broad signal at +24 ppm was detected in the ^{1}H NMR spectrum of **1** in C_6D_6 while the ^{1}H NMR spectrum of **2** displays a very broad peak at +15 ppm. No additional signals could be detected in the range between −100 and +100 ppm.

EPR Spectra of Complexes 1 and 2. The electron paramagnetic resonance (EPR) spectra of [Cp*Fe(η^4-$C_{10}H_8$)] (**1**) and [Cp*Fe(η^4-$C_{14}H_{10}$)] (**2**) reveal rhombic g-tensors characteristic for S = 1/2 systems without any resolved hyperfine coupling (Figure 2). Satisfactory simulations of the experimental spectra were obtained with the g-tensor parameters shown in Table 3. The results of DFT EPR property calculations (Table 3) are in qualitative agreement with the experimental results, giving confidence that the DFT calculated electronic structures are close to the real electronic structures of the compounds.

Magnetic Behavior of Complexes 1 and 2. Complexes [Cp*Fe(η^4-$C_{10}H_8$)] (**1**) and [Cp*Fe(η^4-$C_{14}H_{10}$)] (**2**) are paramagnetic, formally 17e complexes. Their solution effective magnetic moments (Evans' method, C_6D_6 solution) of 1.62 μ_B for **1** and 1.69 μ_B for **2** are close to the theoretical spin-only value of 1.73 μ_B for an S = 1/2 system. Magnetic susceptibility data were also recorded on microcrystalline samples of **1** and **2** in the range of 3−300 K and an external field of 1 kOe. Figure 3 shows that, for both compounds, χT decreases nearly linearly from 300 K down to around 25 K. At lower temperatures, a steep decrease of χT is observed. At 300 K, the χT values are 0.456(1) and 0.460(1) cm^3 K mol^{-1} for **1** and **2**, respectively.

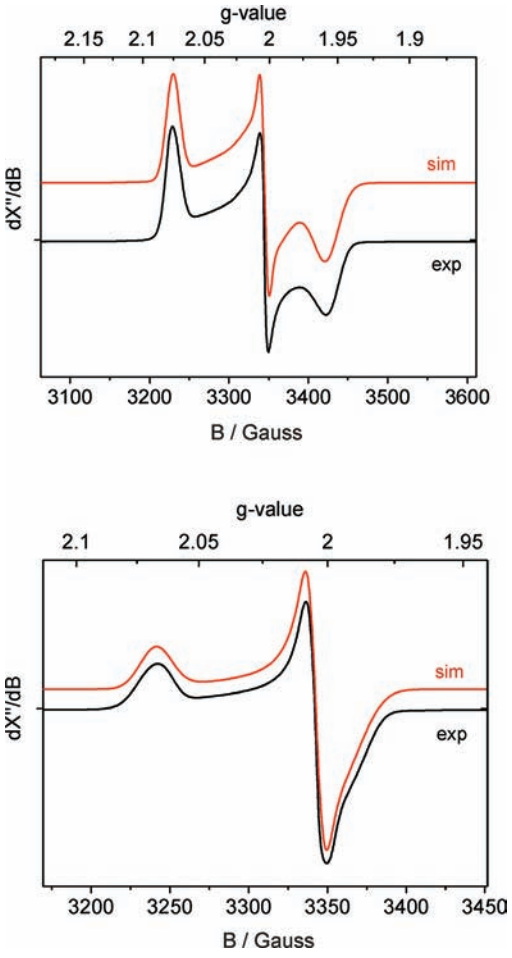

Figure 2. Experimental and simulated X-band EPR spectra of complexes **1** (top) and **2** (bottom). Experimental conditions for **1**: THF/Bu_4NPF_6 glass at 20 K, frequency = 9.380314 GHz, field modulation amplitude = 2 G, microwave power = 0.2 mW. Experimental conditions for **2**: THF glass at 50 K, microwave power 0.2 mW, field modulation amplitude = 2 G, microwave frequency = 9.377730 GHz. The simulated spectra were obtained with the parameters shown in Table 3.

Table 3. Experimental and DFT Calculated EPR Parameters of 1 and 2

		g_{11}	g_{22}	g_{33}	g_{av}[a]
1	Exp.[b]	2.075	2.003	1.958	2.012
	B3LYP, def2-TZVP	2.069	2.019	2.006	2.031
	BP86, def2-TZVP	2.048	2.005	1.992	2.015
2	Exp.[b]	2.067	2.003	1.993	2.021
	B3LYP, def2-TZVP	2.063	2.030	2.006	2.033
	BP86, def2-TZVP	2.049	1.999	1.982	2.010

[a]Average g-value calculated by $g_{av} = (g_1 + g_2 + g_3)/3$. [b]Values obtained from spectral simulations.

The determined effective magnetic moment at 300 K is 1.91(2) μ_B for **1** and 1.92(2) μ_B for **2**. This is somewhat higher than the theoretical spin-only value for an S = 1/2 system which is 1.73 μ_B, corresponding to a χT value of 0.375 cm^3 K mol^{-1}. The latter value is crossed at around 95 K for both compounds.

The fitting of the magnetic susceptibility data was performed using the Curie−Weiss law. This results in a g-factor g = 1.92(1), a Weiss-constant θ = −1.96(5) K and a temperature-independent term χ_{TIP} = 4.2(1) × 10^{-4} cm^3 mol^{-1} for **1**. The

dx.doi.org/10.1021/ic300366m | Inorg. Chem. 2012, 51, 6719−6730

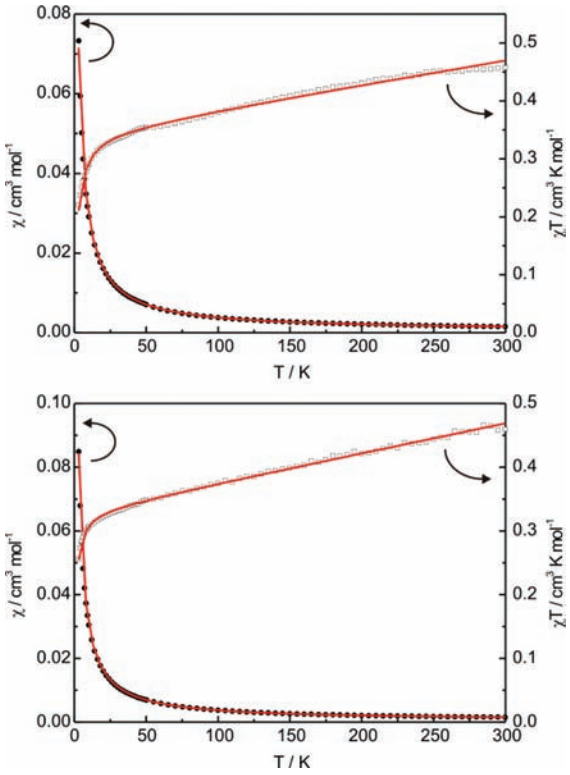

Figure 3. Temperature-dependent magnetic susceptibility (χ and χT data) of **1** (top) and **2** (bottom) measured in a dc-field of 1 kOe. The red lines show the fit of the χ and χT data using the Curie–Weiss law.

same fitting procedure leads to g = 1.87(1), θ = −0.91(3) K, and a temperature-independent term χ_{TIP} = 4.7(1) × 10^{-4} cm^3 mol^{-1} for **2**. The obtained g-factors are lower than the g_{av} = (g_1 + g_2 + g_3)/3 obtained from the EPR measurements (Table 3) presumably because of the presence of diamagnetic impurities in the samples of **1** and **2**. The steep decrease of χT observed below 25 K for both compounds is due to weak intermolecular antiferromagnetic interactions in the solid state.

UV–vis Spectra. The UV–vis spectra of red-brown **K1**, forest green **K2**, dark blue **1**, and dark green **2** were recorded in THF, diethyl ether, and *n*-hexane. The spectra show intense absorptions in the UV region (**K1**: 383 and 414 nm, **1**: 266 and 374 nm, **K2**: 327 and 390 nm, **2**: 274 and 322 nm), which are tentatively assigned to π–π^* transitions in the polyarene ligand.

Weaker absorptions are observed in the visible region (**K1**: 554 nm, **1**: 585 and 755 nm, **K2**: 581 nm, **2**: 627 nm). All visible transitions reveal strong metal-to-ligand charge-transfer (MLCT) character, as assigned on the basis of TD-DFT calculations (see the Supporting Information, Figures S3–S14). The Cp* ligand does not contribute to the CT bands, since the acceptor orbitals are mostly located at the naphthalene/anthracene ligand. Additionally, the bands at 585 nm for **1** and 581 nm for **K2** possess substantial π(M–L)→π^*(M–L) character, that is, a transition between a predominantly naphthalene/anthracene based molecular orbital (MO) showing *bonding* interactions with an iron d-orbital to a similar MO showing *antibonding* interactions (Supporting Information, Figures S7 and S13). The composition of the donor MO and the corresponding acceptor MO for these π(M–L)→π^*(M–L) transitions is nearly identical. This confirms a highly covalent character of the Fe–naphthalene/anthracene bonding. The spectra of the neutral complexes **1** and **2** show weak transitions in the NIR region (**1**: 880 nm, **2**: 825 nm). The band at 880 nm reveals a strong MLCT character with an accepting naphthalene-based π-orbital, whereas the band at 825 nm possesses a strong π(M–L)→π^*(M–L) character.

Redox Properties. Cyclic voltammograms of [Cp*Fe(η^4-$C_{10}H_8$)] (**1**) and [Cp*Fe(η^4-$C_{14}H_{10}$)] (**2**) were recorded in THF at a platinum electrode. The CVs show reversible reduction and oxidation waves assigned to transformation of the neutral complexes to the corresponding monoanions and monocations, respectively (see Supporting Information, Figures S15 and S16).[23] The reductions occur at $E_{1/2}$ = −2.92 V (**1**→$\mathbf{1}^-$) and −2.21 V (**2**→$\mathbf{2}^-$) vs Fc/Fc^+. The reduction **1**→$\mathbf{1}^-$ approaches the reversible behavior only at $\nu \geq 0.5$ V s^{-1}, while the reduction **2**→$\mathbf{2}^-$ is fully reversible.[26] The oxidations are still found at fairly negative potentials, namely, $E_{1/2}$ = −2.03 V (**1**→$\mathbf{1}^+$) and −1.38 V (**2**→$\mathbf{2}^+$) vs Fc/Fc^+. It is noteworthy that the redox potentials of naphthalene complex **1** are significantly more negative than those of anthracene complex **2**. This indicates that complex **2** is harder to oxidize, but more easily reduced than **1**. The observed difference in the redox potentials between complexes **1** and **2** correlates with the different reduction potentials of the free ligands, namely, $E_{1/2}$ = −3.10 V ($C_{10}H_8/C_{10}H_8^{\bullet-}$) and −2.53 V ($C_{14}H_{10}/C_{14}H_{10}^{\bullet-}$) vs Fc/Fc^+.[27]

UV–vis Spectro-Electrochemistry of Complex 2. In addition to the CV study, the UV–vis spectral changes accompanying the *1e* oxidation and *1e* reduction of [Cp*Fe(η^4-$C_{14}H_{10}$)] (**2**) in THF/3 × 10^{-1} M Bu_4NPF_6 on a platinum grid were also monitored in situ by thin-layer spectroelectrochemistry (Figure 4). The characteristic absorptions of **2** at 625 and 825 nm (in THF) disappear during the oxidation. The stable oxidized product [Cp*Fe(η^6-$C_{14}H_{10}$)]$^+$ ($\mathbf{2}^+$) absorbs less intensely in the visible region, showing a broad absorption band with a flat maximum at 570 nm. The UV absorption does not change significantly upon the oxidation.

On the time scale of the spectro-electrochemical experiments (a few minutes), the reduction of **2** proceeded reversibly only at 248 K. The reduction of **2**→$\mathbf{2}^-$ causes new absorption bands to rise at 430 and 640 nm (with apparent shoulders at both sides). The UV–vis absorption spectrum of electrochemically generated $\mathbf{2}^-$ reveals a red shift with respect to the UV-vis absorption recorded for **K2** in Et_2O at 283 K (390 and 581 nm). This shift may be an effect of the formation of an ion-separated structure in THF/Bu_4NPF_6. In nonpolar solvents such as Et_2O the potassium cation might still coordinate to the anthracene ligand as is observed in the solid-state structure of the complex (vide supra).

Mössbauer Spectra. The ^{57}Fe Mössbauer spectra of [K(18-crown-6){Cp*Fe(η^4-$C_{10}H_8$)}] (**K1**), [K(18-crown-6)-{Cp*Fe(η^4-$C_{14}H_{10}$)}] (**K2**), [Cp*Fe(η^4-$C_{10}H_8$)] (**1**), and [Cp*Fe(η^4-$C_{14}H_{10}$)] (**2**) are presented in Figure 5, together with an integral fit of the transmission. The corresponding fitting parameters are listed in Table 4. The spectra were well reproduced by a single quadrupole split signal. Additional signals in the spectra of **1**, **2**, **K1**, and **K2** with an intensity of 23(3), 6(1), 13(1), and 15(4) %, respectively, can be attributed to an impurity phase. We believe that these impurities are due to the high air sensitivity of the compounds which results in some decomposition during the sample preparation and mounting.

The naphthalene complexes **K1** and **1** show isomer shifts of δ = 0.45(1) (**K1**) and δ = 0.65(1) mm s^{-1} (**1**). Somewhat surprisingly, this indicates that the electron density at the nuclei

dx.doi.org/10.1021/ic300366m | Inorg. Chem. 2012, 51, 6719–6730

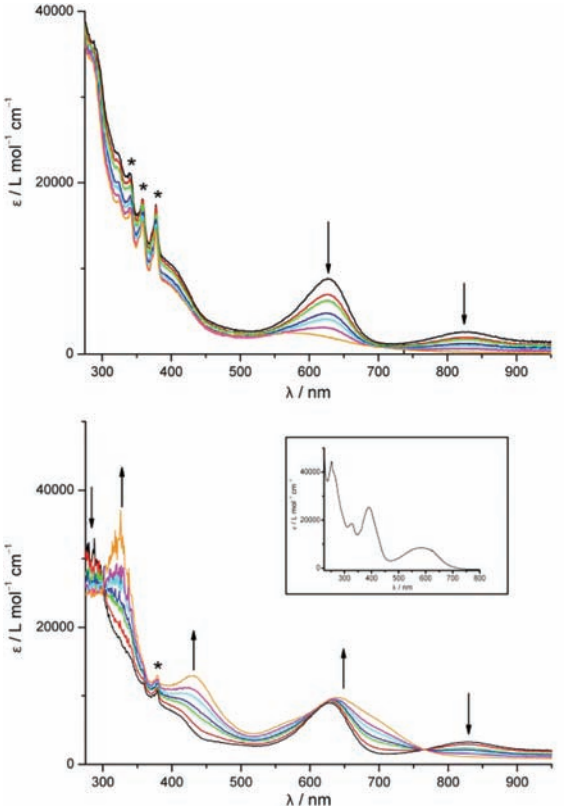

Figure 4. UV−vis spectral changes accompanying the reversible oxidation **2**→**2**$^+$ (top) and the reduction **2**→**2**$^-$ (bottom) on a Pt grid in THF/Bu_4NPF_6 at 248 K within an OTTLE cell. The arrows show the intensity changes during the potential ramping to the oxidation or reduction potentials of **2**. The asterisks indicate the absorptions of free anthracene formed during the spectro-electrochemical experiment because of partial decomposition of complex **2**. The inset shows the UV−vis spectrum of complex **K2** in Et_2O.

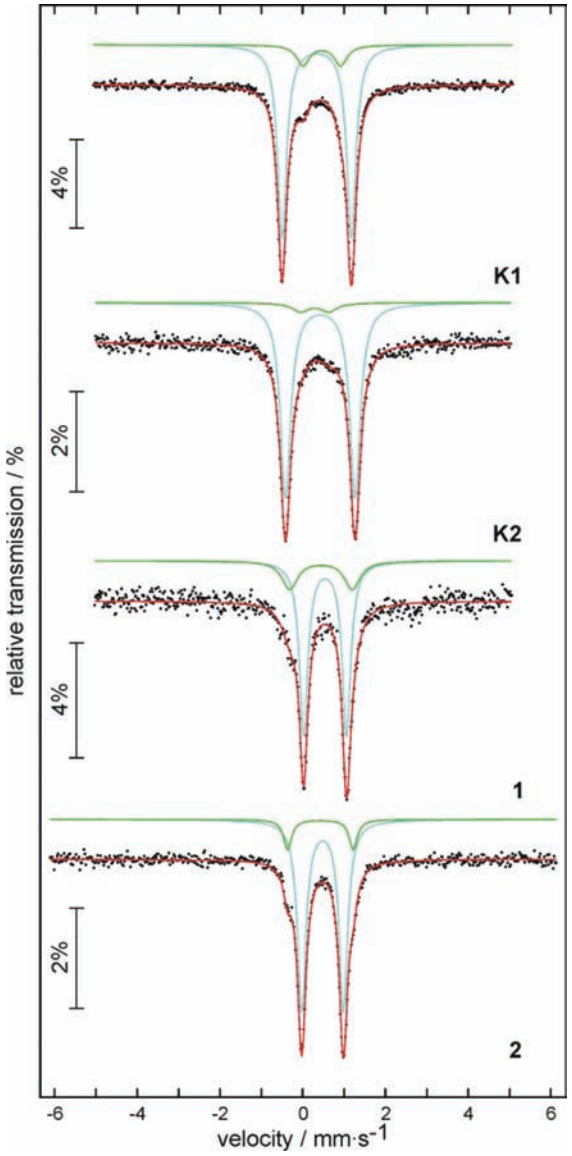

Figure 5. Experimental (data points) and simulated (continuous lines) ^{57}Fe Mössbauer spectra of **K1**, **K2**, **1**, and **2** at 78 K.

is higher in the oxidized complex **1** compared to the reduced **K1**. The anthracene complexes **K2** and **2** show nearly identical isomer shifts of δ = 0.54(1) (**K2**) and 0.59(1) mm s^{-1} (**2**), which indicates that the electron density at the nuclei is very similar in both complexes. The noncubic site symmetry is reflected in quadrupole splittings of ΔE_Q = 1.68(1) (**K1** and **K2**), 1.04(1) (**1**), and 1.01(1) mm s^{-1} (**2**), respectively.

The isomer shifts and quadrupole splittings for the complexes $\mathbf{1}^{-/0/+}$ and $\mathbf{2}^{-/0/+}$ were also calculated at the B3LYP level of theory. The calculated values are given in Table 4 and show a reasonable agreement with the experimental data for **K1**, **K2**, **1**, and **2**. The observed differences in the calculated and the experimental quadrupole splitting constants are likely due to differences between calculated and experimental Fe−C(ligand) bond distances.

Population Analyses. DFT calculations were performed at the B3LYP level to analyze the electronic structures of the complexes $[Cp^*Fe(C_{10}H_8)]^{-/0/+}$ ($\mathbf{1}^{-/0/+}$) and $[Cp^*Fe(C_{14}H_{10})]^{-/0/+}$ ($\mathbf{2}^{-/0/+}$). Note that both the iron atoms and the naphthalene or anthracene ligands are potentially redox active. Thus, to distinguish between ligand-based and metal-based redox events within the series $\mathbf{1}^{-/0/+}$ and $\mathbf{2}^{-/0/+}$, we employed an analysis of reduced orbital charges and orbital spin densities.[28] Such an analysis provides information about the electron and spin populations for each metal d-orbital.

Table 4. Calculated and Experimental ^{57}Fe Mössbauer Spectroscopic Parameters for the $\mathbf{1}^{-/0/+}$ and $\mathbf{2}^{-/0/+}$ Redox Series Obtained from Spin-Unrestricted B3LYP-DFT Calculations[a]

compound	δ (mm s^{-1})[b]	ΔE_Q (mm s^{-1})[c]	η[d]
$\mathbf{1}^+$	0.606	+2.363	0.22
1	0.621 [0.65(1)]	−1.427 [1.04(1)]	0.83
$\mathbf{1}^-$	0.498 [0.45(1)]	+2.468 [1.68(1)]	0.81
$\mathbf{2}^+$	0.606	+2.406	0.33
2	0.576 [0.59(1)]	+1.658 [1.01(1)]	0.53
$\mathbf{2}^-$	0.559 [0.54(1)]	+2.558 [1.68(1)]	0.74

[a]CP(PPP) basis set for iron. Experimental values for **K1**, **K2**, **1**, and **2** at 78 K are given in square brackets. [b]Relative to metallic iron at room temperature. [c]Electric quadrupole splitting. [d]Asymmetry parameter $\eta = (V_{xx} - V_{yy})/V_{zz}$.

Thus, a charge population of 2 and a spin population of 0 are benchmarks for a fully occupied d-orbital. A charge population of 1 and a spin population of 1 indicate a singly occupied

dx.doi.org/10.1021/ic300366m | Inorg. Chem. 2012, 51, 6719−6730

Table 5. Reduced Orbital Charges and Orbital Spin Densities[a]

	1^+		1		1^-		2^+		2		2^-	
	charge	spin	charge	spin	charge	spin	charge	spin	charge	spin	charge	spin
d_{z^2}	1.96	0.0	1.93	0.01	1.91	0.0	1.95	0.0	1.94	0.01	1.92	0.0
d_{xz}	0.92	0.0	0.85	0.06	0.82	0.0	0.93	0.0	0.89	0.04	0.81	0.0
d_{yz}	0.90	0.0	1.15	0.44	1.09	0.0	0.89	0.0	1.08	0.32	1.08	0.0
$d_{x^2-y^2}$	1.63	0.0	1.43	0.31	1.75	0.0	1.61	0.0	1.53	0.18	1.74	0.0
d_{xy}	1.74	0.0	1.75	0.03	1.61	0.0	1.76	0.0	1.73	0.02	1.64	0.0
Σd_i	7.15	0.0	7.11	0.86	7.18	0.0	7.15	0.0	7.17	0.57	7.19	0.0
Fe_{total}[b]		0.0		0.89		0.0		0.0		0.59		0.0
L_{total}[c]		0.0		0.11		0.0		0.0		0.41		0.0

[a]Spin-unrestricted B3LYP-DFT calculations, Löwdin population analysis. The *z*-axis is defined as a vector pointing from a metal ion towards the center of a Cp* ligand, whereas the *y*-axis is chosen to point along a naphthalene or anthracene ligand. [b]Total spin density on iron including s- and p-orbitals. [c]Total spin density on the ligands.

molecular orbital (SOMO), whereas the charge and spin populations are both 0 for unoccupied orbitals. The populations in transition metal complexes can in practice deviate from the given ideal values because of covalency and spin-polarization effects, but the trends are easy to follow.[28] We begin our analysis with the diamagnetic cations $\mathbf{1}^+$ and $\mathbf{2}^+$.[14] Both $\mathbf{1}^+$ and $\mathbf{2}^+$ show large (>1.6) charge populations for the d_{z^2}, $d_{x^2-y^2}$, and d_{xy} iron orbitals, but small (<1.0) charge populations for d_{xz} and d_{yz} orbitals. These values point to the doubly occupied nature of the former and the essentially unoccupied nature of the latter orbitals (Table 5). Similarly to the situation in ferrocene, the d_{xz} and d_{yz} orbitals of the Fe^{II} ion in $\mathbf{1}^+$ and $\mathbf{2}^+$ are significantly destabilized through the π-type antibonding interactions with the ligand orbitals and hence remain unoccupied (Supporting Information, Figure S17).

The neutral species **1** and **2**, which are the products of the one-electron reduction of $\mathbf{1}^+$ and $\mathbf{2}^+$, possess a spin-doublet ($S = 1/2$) ground state. The Löwdin population analyses revealed a spin population of 0.89 on iron for the naphthalene complex **1** and 0.59 for the anthracene complex **2**. The remaining fractions of the unpaired electron density are distributed predominantly over the polyarene ligands (Figure 6). The metal-based *spin density* is mainly localized in the d_{yz} orbital (**1**: 0.44, **2**: 0.32) and, to a lesser extent, in the $d_{x^2-y^2}$ orbital (**1**: 0.31, **2**: 0.18). Note that the *charge density* in the d_{yz} orbital

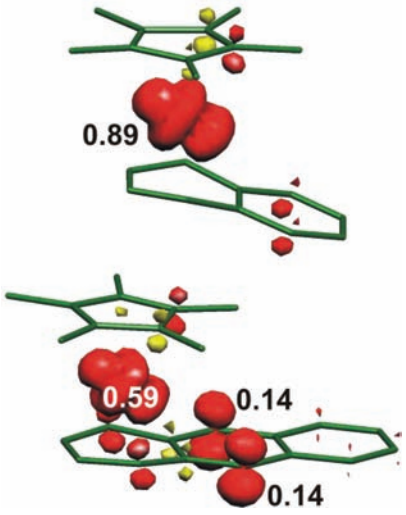

Figure 6. Spin density map for **1** (top) and **2** (bottom) obtained from the spin-unrestricted B3LYP-DFT calculations.

significantly increases upon reduction by 0.25 electrons ($\mathbf{1}^+ \rightarrow \mathbf{1}$) and 0.19 electrons ($\mathbf{2}^+ \rightarrow \mathbf{2}$), respectively. The reductions of the neutral complexes **1** and **2** to the monoanionic species $\mathbf{1}^-$ and $\mathbf{2}^-$ result in significant changes in the charge population. The charge population at the formally fully occupied $d_{x^2-y^2}$ orbital in **1** (1.43 electrons) significantly increases in the reduced monoanion $\mathbf{1}^-$ (1.75 electrons). This increase is compensated by the decrease of the charge density at the other iron d-orbitals, however. Similarly, the reduction $\mathbf{2} \rightarrow \mathbf{2}^-$ results in an increase of the population at the $d_{x^2-y^2}$ by 0.21 electrons.

DISCUSSION

Although cationic and neutral polyarene complexes $[CpFeL]^+$ and $[CpFeL]$ (Cp = cyclopentadienyl derivative, L = polyarene) have attracted continuous interest over the years,[14,29,30] very little was known about $[CpFeL]^-$ anions prior to this work.[17] The reaction of $Cp^*Li/FeCl_2(thf)_{1.5}$ with potassium naphthalenide now provides a convenient route to the synthetically valuable complex $[K(18\text{-crown-}6)\{Cp^*Fe(\eta^4\text{-}C_{10}H_8)\}]$ (**K1**, Scheme 1). The same approach is less fruitful for the anthracene derivative $[K(18\text{-crown-}6)\{Cp^*Fe(\eta^4\text{-}C_{14}H_{10})\}]$ (**K2**). However, the desired complex is accessible from **K1** via ligand exchange (Scheme 2a). In addition to the synthesis of the anionic complexes **K1** and **K2**, we could access the neutral complexes $[Cp^*Fe(\eta^4\text{-}C_{10}H_8)]$ (**1**) and $[Cp^*Fe(\eta^4\text{-}C_{14}H_{10})]$ (**2**, Schemes 1 and 2) as well. Complex **1** was isolated by oxidation of anion $\mathbf{1}^-$. Somewhat surprisingly, complex **2** was reproducibly isolated from the 2:1 reaction of potassium anthracenide with "Cp*FeCl" in the absence of crown ether. While the reason for this observation is not entirely clear, a possible explanation might be an equilibrium (Scheme 3)

Scheme 3. Proposed Equilibrium of the Anthracene Complexes 2^- and 2 in the Reaction Mixture

$$\underset{\mathbf{2}^-}{[Cp^*Fe(\eta^4\text{-}C_{14}H_{10})]^-} + C_{14}H_{10} \rightleftharpoons \underset{\mathbf{2}}{[Cp^*Fe(\eta^4\text{-}C_{14}H_{10})]} + C_{14}H_{10}^{\bullet-}$$

between $\mathbf{2}^-$, **2**, anthracene, and the anthracenide anion in solution, which could be formed because of the comparably negative reduction potentials of complex **2** ($E_{1/2} = -2.21$ V vs Fc/Fc^+) and anthracene ($E_{1/2} = -2.53$ V vs Fc/Fc^+). Although this equilibrium should be shifted to the left side in solution, it could depend on the crystallization conditions if anionic $\mathbf{2}^-$ or neutral **2** is isolated.

Cyclic voltammetry of **1** and **2** and, in the case of **2**, spectroelectrochemical experiments show that these neutral complexes

dx.doi.org/10.1021/ic300366m | Inorg. Chem. 2012, 51, 6719−6730

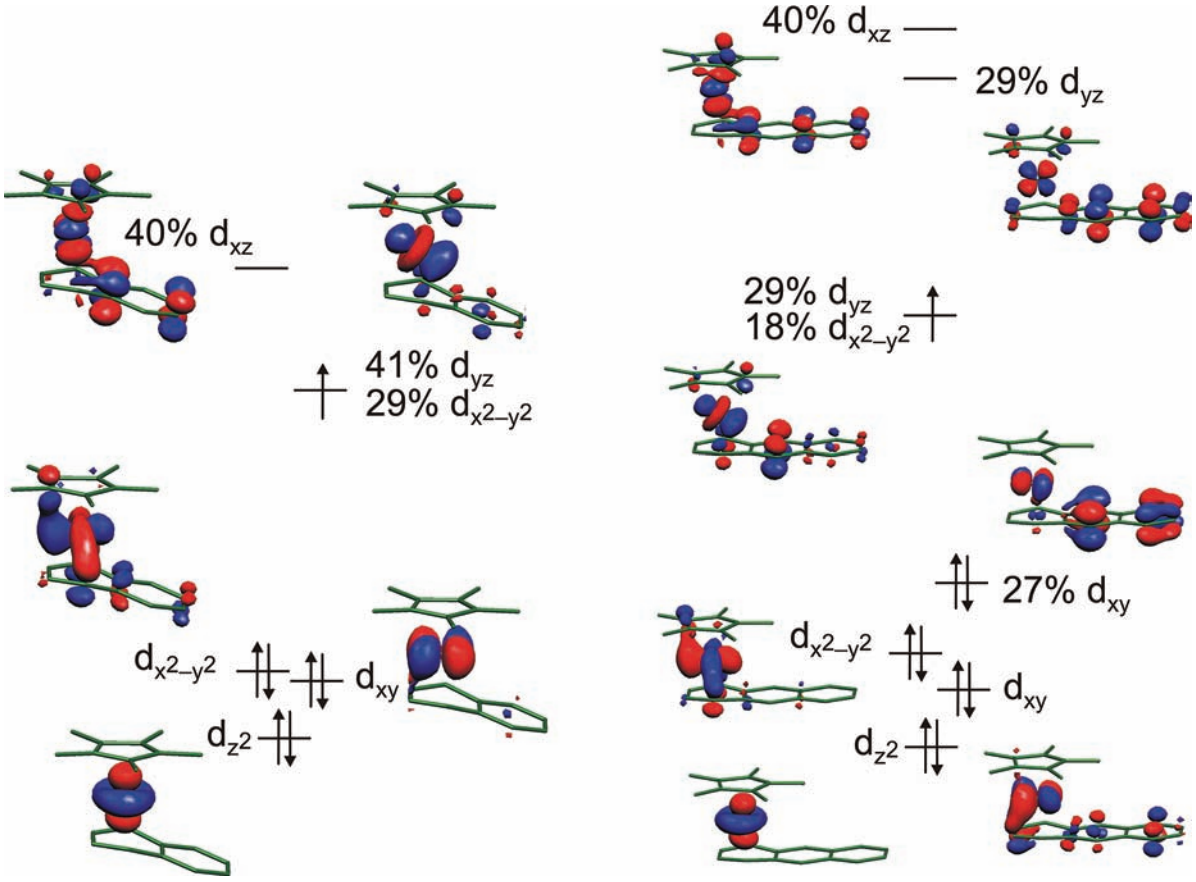

Figure 7. Quasi-restricted frontier orbitals for **1** (left) and **2** (right) obtained from the spin-unrestricted B3LYP-DFT calculations. The *z*-axis is defined as a vector pointing from a metal ion toward the center of a Cp* ligand, whereas the *y*-axis is chosen to point along a naphthalene or anthracene ligand.

can be reversibly oxidized to the cations $[Cp^*Fe(\eta^6\text{-}C_{10}H_8)]^+$ $(\mathbf{1}^+)$[14,23] and $[Cp^*Fe(\eta^6\text{-}C_{14}H_{10})]^+$ $(\mathbf{2}^+)$ and reversibly reduced to the anionic complexes $[Cp^*Fe(\eta^4\text{-}C_{10}H_8)]^-$ $(\mathbf{1}^-)$ and $[Cp^*Fe(\eta^4\text{-}C_{10}H_8)]^-$ $(\mathbf{2}^-)$ at low temperatures.

The frontier molecular orbitals of both complexes are displayed in Figure 7. Ligand π^*-orbitals obviously contribute significantly to the SOMOs of both complexes. This partial ligand character of the frontier orbitals determines the substantial variation of the redox potentials of **1** and **2**, which are significantly more negative for the naphthalene derivative.

The synthesis of complexes **K1**, **K2**, **1**, and **2** presents a unique opportunity to examine the effect of reduction and oxidation on the structures, spectroscopic features, and the electronic situation in a series of low-valent naphthalene and anthracene complexes. The $[Cp^*FeL]^{-/0/+}$ complexes investigated here contain the metal center in the *formal* oxidation states 0 to +II, respectively. Assigning the *spectroscopic* oxidation state of the metal atom is a more difficult and complex issue, however. To the best of our knowledge, such a study has not been attempted before for highly reduced, polyarene transition metalates.

According to our DFT calculations, the electronic structures of the cations $\mathbf{1}^+$ and $\mathbf{2}^+$ are best described as low-spin Fe^{II} ions coordinated to the Cp* anion and the neutral naphthalene or anthracene ligand (Chart 2, configuration I). In contrast, the electronic structures of the neutral complexes **1** and **2** may be represented by the two resonance configurations II and III displayed in Chart 2. Configuration II shows a low-spin Fe^{I} ion

Chart 2

$[Cp^{*-I}Fe^{+II}L^0]^+$ **I**	$L = C_{10}H_8, C_{14}H_{10}$
$[Cp^{*-I}Fe^{+I}L^0]$ **II**	$[Cp^{*-I}Fe^{+II}L^{-I}]$ **III**
$[Cp^{*-I}Fe^{+II}L^{-II}]^-$ **IV**	$[Cp^{*-I}Fe^{+I}L^{-I}]^-$ **V**

coordinated to a neutral naphthalene or anthracene ligand L, while configuration III represents a low-spin Fe^{II} ion (d^6 electronic configuration) coordinated to a radical anionic ligand $L^{\bullet-}$. In the latter description, the presence of a naphthalene or anthracene radical anion is required. Interestingly, the EPR spectra of the paramagnetic complexes **1** and **2** reveal relatively small *g*-anisotropies of the rhombic *g*-tensors, which is frequently associated with a substantial ligand radical character.[31] However, an alternative explanation for the observed small *g*-anisotropies is a large energy separation between the spin-bearing d-orbital in the SOMO and the d-orbitals of appropriate symmetry for spin−orbit coupling with the SOMO, thus reducing the probability of spin−orbit coupling effects.[31]

Astruc and co-workers already predicted for **1** that about 15−30% of the spin density is localized on the ligand on the basis of electrochemical measurements (Vlcek's theory).[14,32] Our DFT calculations on **1** show 89% of the spin density to be located at iron, with a small part present on the naphthalene ligand

dx.doi.org/10.1021/ic300366m | *Inorg. Chem.* 2012, 51, 6719−6730

(Figure 6 and Table 5). In complex **2**, a larger portion (41%) of the unpaired spin density is localized on the ligands. This difference points to a stronger contribution of the Fe^{I} configuration II to the electronic structure of **1** compared to **2**, which can be qualitatively explained by the fact that the redox-active π-orbital of the naphthalene ligand is higher in energy than the corresponding orbital of the larger anthracene ligand. Hence, the redox-active orbital of naphthalene is less accessible for reduction. As a result, complex **1** shows a pronounced metal-based radical character. Nevertheless, the small *g*-anisotropy and the significant folding of the coordinating C_6-ring of the naphthalene ligand in **1** (20.0°) point to a contribution of resonance structure III, containing a monoanionic naphthalene radical ligand coordinated to Fe^{II} for **1**.

Note that although simple examination of the frontier quasi-restricted orbitals points to a low-spin Fe^{I} ion in **1**, inspection of the frontier MOs in **2** is less informative because of the more delocalized nature of these MOs and stronger covalence effects in **2** (Figure 7).

The Löwdin population analysis (Table 5) furthermore reveals similar changes in the reduced orbital charges accompanying the reductions **1**→**1**$^-$ and **2**→**2**$^-$: The most notable differences between the neutral species **1** and **2** and the reduced monoanions **1**$^-$ and **2**$^-$ are the increase of the charge population at the $d_{x^2-y^2}$ orbital in the anions by about 0.2 electrons (Table 5). This increase is, however, compensated by the decrease of the charge density at other iron d-orbitals. The reduced character of the naphthalene and anthracene ligands in the anions is apparent in the strong folding of the metal-coordinated C_6-ring of 38.2° in **1**$^-$ and 31.6° in **2**$^-$, which is a sign of an increased metal to ligand back-bonding in the diamagnetic anions **1**$^-$ and **2**$^-$. These anions are thus best described as low-spin Fe^{II} ions coordinated to a dianionic naphthalene or a dianionic anthracene ligand L^{2-}, respectively (Chart 2, configuration IV). An alternative description of the electronic structure would be a low-spin Fe^{I} ion that is antiferromagnetically spin-coupled to a monoanionic naphthalene or anthracene radical $L^{\bullet-}$ (configuration V); however, we did not find any evidence for such a scenario.

An additional probe for the oxidation and spin states of the iron centers in **1**$^{-/0/+}$ and **2**$^{-/0/+}$ are the ^{57}Fe Mössbauer spectroscopic parameters. The calculated values for the isomer shift and quadrupole splittings are in good agreement with the experimental data (Table 4). It is very important to note that, except for the **1**$^+$→**1** pair, the calculated isomer shift slightly and gradually *decreases* on each reduction step for both series **1**$^{-/0/+}$ and **2**$^{-/0/+}$. However, an *increase* of the isomer shift is expected if the iron atom is reduced.[33] This indicates that the redox events within the **1**$^{-/0/+}$ and **2**$^{-/0/+}$ redox series are predominantly ligand-centered. While the calculated isomer shifts decrease steadily for the anthracene series from the cation **2**$^+$ (0.606 mm s^{-1}) via neutral **2** (0.576 mm s^{-1}) to the anion **2**$^-$ (0.559 mm s^{-1}), the calculated isomer shift for the neutral naphthalene complex **1** (0.621 mm s^{-1}) is larger than for the oxidized complex **1**$^+$ (0.606 mm s^{-1}). It is also much larger than the isomer shift for the reduced monoanion **1**$^-$ (0.498 mm s^{-1}). The exceptionally large isomer shift for complex **1** confirms the significant Fe^{I} character of this species that we derived from the DFT calculations. A further hint for the dominating low-spin Fe^{I} electronic configuration of the metal atom in **1** is the quadrupole splitting. The complexes **1**$^-$, **1**$^+$, and **2**$^{-/0/+}$ each have similar and positive quadrupole splitting constants that point to a similar low-spin Fe^{II} configuration (Table 4). In contrast, compound **1** is the only complex in the series that shows a negative sign of the quadrupole splitting constant.

CONCLUSIONS

The reduction of Cp*Li/$FeCl_2(thf)_{1.5}$ with potassium naphthalenide and potassium anthracenide opens a viable, new route toward the low-valent naphthalene and anthracene iron complexes [K(18-crown-6){Cp*Fe(η^4-$C_{10}H_8$)}] (**K1**), [Cp*Fe(η^4-$C_{10}H_8$)] (**1**), [K(18-crown-6){Cp*Fe(η^4-$C_{14}H_{10}$)}] (**K2**), and [Cp*Fe(η^4-$C_{14}H_{10}$)] (**2**). We expect that these complexes will be promising reagents for future synthetic and catalytic applications, and their potential as sources of the "Cp*Fe$^-$" and "Cp*Fe" synthons is currently being investigated.[16] The structural, spectroscopic and DFT studies performed here show that the *formal* oxidation state of iron in the anionic, neutral, and cationic complexes [Cp*Fe(L)]$^{-/0/+}$ (L = $C_{10}H_8$, $C_{14}H_{10}$) varies between 0 and +II, but the *spectroscopic* oxidation state is close to +II in all cases except for the naphthalene complex **1**, which shows substantial Fe^{I} character. Naphthalene and anthracene thus behave as redox noninnocent ligands *par excellence* in the investigated complexes, and probably many other metalates.[1−7]

EXPERIMENTAL SECTION

General Procedures. All procedures were carried out under an inert atmosphere of purified argon. Solvents were dried over sodium (*n*-pentane, *n*-hexane, *n*-heptane) or sodium/benzophenone (DME, THF, diethylether) and distilled under argon prior to use. Cp*Li, $FeCl_2(thf)_{1.5}$ and Cp*FeCl(tmeda) were prepared according to the literature procedures.[34] $C_{10}H_8$, $C_{14}H_{10}$, and AgOTf were obtained commercially and used as received. 18-Crown-6 was purified by vacuum sublimation before use. ^{1}H and ^{13}C{^{1}H} NMR spectra were recorded on a Bruker Avance 400 spectrometer (400.13 and 100.59 MHz). ^{1}H and ^{13}C{^{1}H} NMR signals were referenced internally to residual solvent signals. EI MS spectra were recorded on a Varian MAT 212 spectrometer. UV−vis spectra were recorded on a Hewlett-Packard G1103A spectrophotometer. Melting points were obtained in sealed glass capillaries under argon using a Stuart Scientific melting point apparatus and are uncorrected. The numbering scheme of the hydrogen and carbon atoms of complexes **K1** and **K2** follows the labeling in Figure 1.

[K(18-crown-6){Cp*Fe(η^4-$C_{10}H_8$)}] (K1). A cooled solution (−30 °C) of CpLi* (2.35 g, 10 mmol) and $FeCl_2(thf)_{1.5}$ (1.42 g, 10 mmol) in DME (60 mL) was added to a dark-green DME solution (150 mL) of $KC_{10}H_8$ (20 mmol) and 18-crown-6 (2.96 g, 11 mmol) at −78 °C. The mixture turned orange-red immediately and was warmed to −30 °C. After filtration and concentration of the mother liquor to 80 mL, *n*-hexane (80 mL) was added to precipitate **K1** (3.55 g, 57%) as a dark-brown microcrystalline solid. mp 168−170 °C (dec to a dark oil). ^{1}H NMR (400.03 MHz, THF-d_8, 230 K): δ 0.42 (br, 2H, $H_{11,14}$), 1.71 (br, overlapping with solvent signals, 15H, Cp*,), 3.56 (br, overlapping with solvent signals, 24H, 18-crown-6), 4.80 (br, 2H, $H_{12,13}$), 5.21 (overlapping m, 2H, $H_{15,18}$ or $H_{16,17}$), 5.30 (overlapping m, 2H, $H_{15,18}$ or $H_{16,17}$); ^{13}C{^{1}H} NMR (100.59 MHz, THF-d_8, 200 K): δ 12.8 (CCH_3 of Cp*), 44.9 ($C_{11,14}$), 71.2 (18-crown-6), 72.4 ($C_{12,13}$), 77.5 (CCH_3 of Cp*), 114.5 ($C_{15,18}$ or $C_{16,17}$), 117.4 ($C_{15,18}$ or $C_{16,17}$), 157.0 ($C_{19,20}$); UV−vis (THF, λ_{max}/nm (ε_{max}/dm^3 mol^{-1}cm^{-1})): 383, 414 (shoulders), 554 (2100). Satisfactory elemental analysis could not be obtained because of the extreme sensitivity of the compound.

[K(18-crown-6){Cp*Fe(η^4-$C_{14}H_{10}$)}] (K2). Complex **K1** (0.632 g, 1.02 mmol) and anthracene (0.272 g, 1.52 mmol) were dissolved in 40 mL of THF at −40 °C. The reaction mixture was allowed to warm up to room temperature (r.t.) and stirred for two weeks. During that time the red orange solution turned slowly forest green. After evaporating the solvent, naphthalene was removed through sublimation. The residue was washed with *n*-pentane, redissolved in THF (15 mL), and

dx.doi.org/10.1021/ic300366m | Inorg. Chem. 2012, 51, 6719−6730

layered with *n*-pentane (15 mL). Dark green crystals of **K2** (0.109 g, 16%) formed at −18 °C. mp 156−158 °C (dec.). ^{1}H NMR (400.13 MHz, toluene-d_8, 190 K): δ 1.6 (br, 2H, $H_{11,14}$), 2.3 (br s, 15H of Cp*), 3.2 (br s, 24H of 18-crown-6), 4.6 (br, 2H, $H_{12,13}$), 5.3 (br, 2H, $H_{19,20}$), 6.2/6.5 (br m, 4H, $H_{15,16,17,18}$). ^{13}C NMR (100.61 MHz, toluene-d_8, 190 K): δ 11.8 ($C_5(CH_3)_5$), 51.2 ($C_{11,14}$), 72.9 ($C_{12,13}$), 80.1 ($C_5(CH_3)_5$), 97.2 ($C_{19,20}$), 120.6 ($C_{15,16,17,18}$), 137.1 (overlapping with solvent signal, $C_{23,24}$), 144.1 ($C_{21,22}$). UV−vis (Et_2O, λ_{max}/nm (ε_{max}/dm^3 mol^{-1} cm^{-1})): 327 (18500), 390 (25500), 581 (8500). Elemental analysis for $C_{36}H_{49}O_6FeK$ (672.7): calcd.: C 64.27, H 7.34; found: C 63.61, H 7.16.

[Cp*Fe(η^4-$C_{10}H_8$)] (1). A solution of AgOTf (0.513 g, 2.00 mmol) in THF (30 mL) was added slowly to a THF solution of **K1** (1.245 g, 2.00 mmol) at −78 °C. The suspension turned dark blue immediately and was allowed to warm to room temperature overnight. After filtration and removal of the solvent in vacuo, the residue was extracted with *n*-hexane (80 mL). Needle like crystals of **1** (0.299 g, 47%) formed on storage of the solution at −18 °C for several days. mp 101−103 °C (dec.). Magnetic susceptibility (Evans' NMR method, benzene-d_6): μ_{eff} = 1.69 μ_B. ^{1}H NMR (200.13 MHz, benzene-d_6, 300 K): δ 24 (very br); UV−vis (*n*-hexane, λ_{max}/nm, (ε_{max}/dm^3 mol^{-1}cm^{-1})): 266 (23000), 293 (shoulder), 374 (4000), 585 (3000), 755 (1500), 880 (1000). EI MS (*m*/*z* (%)): 326 (6.4, Cp*$_2$Fe), 319 (72.4, **1**), 189 (6.0, C_5Me_5Fe−2H), 128 (100.0, $C_{10}H_8$). Elemental analysis for $C_{20}H_{23}Fe$ (319.2): calcd.: C 75.25, H 7.26; found C 74.80, H 7.25.

[Cp*Fe(η^4-$C_{14}H_{10}$)] (2). A solution of Cp*Fe(tmeda)Cl (1.000 g, 2.91 mmol) in 15 mL of THF was added to a stirred solution of $KC_{14}H_{10}$ (5.67 mmol) in 70 mL of THF at −78 °C. The deep blue $KC_{14}H_{10}$ solution turned green during the addition. After 12 h stirring and warm-up to r.t., the solvent was removed in vacuum and the residue was washed with *n*-heptane (3 × 30 mL). The solid was redissolved in 90 mL of diethyl ether. The lime green solution was filtered, concentrated to 20 mL and layered with 20 mL of *n*-hexane. At −18 °C dark green block shaped crystals of **2** (0.246 g, 24%) precipitated. mp 119−120 °C (dec.). Magnetic susceptibility (Evans' NMR method, benzene-d_6): μ_{eff} = 1.62 μ_B. ^{1}H NMR (400.03 MHz, benzene-d_6, 300 K): δ 10−20 (br, Cp*); UV−vis (Et_2O, λ_{max}/nm, (ε_{max}/dm^3 mol^{-1} cm^{-1})): 274 (38500), 322 (22500), 627 (9000). EI MS (*m*/*z* (%)): 369 (10.6, **2**), 326 (3.5, Cp*$_2$Fe), 178 (100.0, $C_{14}H_{10}$), 135 (8.8, Cp*), 119 (5.1). Elemental analysis for $C_{24}H_{25}Fe$ (369.3): calcd.: C 78.05, H 6.82; found: C 77.92, H 6.67.

X-ray Crystallography. The crystallographic data of **K2** and **2** (Table 6) were collected on a Bruker APEXII diffractometer equipped with a rotating anode (Mo-K_α radiation, λ = 0.71073 Å). The crystals were coated with paratone oil, and mounted on a glass fiber in the cooled nitrogen stream of the diffractometer. All data were collected at 153(2) K. The crystallographic data of **K1** have been previously communicated.[16a]

EPR Spectroscopy. Experimental X-band EPR spectra were recorded on a Bruker EMX spectrometer equipped with a He temperature control cryostat system (Oxford Instruments). The spectra were simulated by iteration of the anisotropic *g*-values, (super)hyperfine coupling constants, and line widths using the W95EPR program (available upon request from Prof. Frank Neese, MPI for Bioninorganic Chemistry, Mülheim).

Magnetic Measurements. A 14.3 mg portion of **1** and 10.7 mg of **2** were packed in polypropylene capsules under an inert-gas atmosphere and sealed with Teflon tape. The capsules were attached to a sample holder rod of a Quantum Design Physical-Property-Measurement-System. The magnetic measurements were performed using the VSM option. The samples were measured in a zero-field cooled mode in the range of 3−300 K with an applied field of 1 kOe. At each measurement point a waiting period of 300 s was imposed to allow for thermal equilibration of the samples. A diamagnetic correction was applied to compensate for the capsule and Teflon tape, by performing a reference measurement. Additionally diamagnetic corrections to the magnetic susceptibilities were applied using the increments by Haberditzl.[35] Fitting of the magnetic data was performed using the following Curie−Weiss equation: $\chi = (C/(T - \theta_p)) + \chi_{TIP}$ where $C = ((N_A g^2 \mu_B^2)/(4k_B))$ for a spin-only system with S = 1/2.

Table 6. Structural Data of K2 and 2[a]

	K2	2
empirical formula	$C_{36}H_{49}FeKO_6$	C_{24} H_{25} Fe
M	672.70	369.29
crystal system	monoclinic	orthorhombic
space group	$P2_1/c$	$Pca2_1$
a/Å	19.6401(14)	15.5887(10)
b/Å	17.6383(12)	7.9705(5)
c/Å	22.0480(16)	15.1076(9)
β/deg	116.4140(10)	90
V/Å^3	6840.5(8)	1877.1(2)
Z	8	4
ρ_{calcd}/g·cm^{-3}	1.31	1.31
θ_{max}/deg	27.88	29.61
total data	67584	20394
unique data (R_{int})	16254 (0.0261)	5275 (0.0273)
parameters (restraints)	800 (0)	271 (1)
goodness of fit on F^2	1.033	1.030
*R*1, *wR*2 [$I > 2\sigma(I)$]	0.0315, 0.0792	0.031, 0.0727
*R*1, *wR*2 (all data)	0.0461, 0.0882	0.0383, 0.0771
Flack parameter		0.004(12)
largest diff. peak and hole/e·Å^{-3}	0.51 and −0.45	0.32 and −0.72

[a]Programs SHELXL, SHELXL-97;[36] solutions using the Patterson method, full matrix refinement with all independent structure factors.

Cyclic Voltammetry. Cyclic voltammograms of **1** were recorded with a Metrohm Autolab potentiostat PGSTAT302 operated by the Nova software (Version 1.6.013) with *i*R-Compensation (R = 1.2 kΩ). A temperature controlled airtight electrochemical cell (Fa. Halbmikrotechnik Chemie) containing a 3 mm diameter Pt working electrode (polished with 1.00 μm diamond paste and 0.05 μm aluminum oxide paste), a Pt coil auxiliary electrode (separated by a D4 glass frit), and an Ag/AgOTf reference electrode with Haber−Luggin capillary was used.

The cyclic voltammogram of **2** was recorded with an EG&G PAR Model 283 potentiostat with the Power CV software. A single-compartment airtight electrochemical cell was equipped with a 0.14 mm^2 Pt microdisc working electrode (polished with 0.25 μm diamond paste from Oberflächentechnologien Ziesmer), a Pt wire auxiliary electrode, and an Ag wire pseudoreference electrode.

UV−vis Spectroelectrochemistry. The in situ UV−vis monitoring of the redox reactions of complex **2** (in THF/3 × 10^{-1} M Bu_4NPF_6) in the temperature range 293−248 K was carried out with an OTTLE cell positioned in the sample compartment of a Scinco S3100 diode array spectrophotometer.[37] The Pt minigrid working electrode potential was controlled with a PA4 potentiostat (Laboratory Devices, Polná, Czech Republic).

Mössbauer Spectroscopy. A ^{57}Co/Rh source was available for the ^{57}Fe Mössbauer spectroscopic investigations. The samples were placed in thin-walled PMMA containers which were sealed with an epoxy resin. The measurements were performed in the usual transmission geometry at 78 K. Fitting of the spectra was performed using the NORMOS-90 program system.[38]

Mass Spectrometry. EI MS spectra were recorded on a Varian MAT 212 spectrometer.

Quantum Chemical Calculations. Geometry optimizations of **1**$^-$, **1**, **1**$^+$, **2**$^-$, **2**, and **2**$^+$ were performed using the TURBOMOLE program system.[39] The BP86 density functional and the def2-TZVP basis set were employed for all atoms, and the RI approximation was used.[20−22] For the electronic structures and Mössbauer spectroscopic parameters, single point calculations were then performed on the optimized geometries using the program package ORCA. For the EPR calculations, the geometries of the full atom model of **1** and **2** were

dx.doi.org/10.1021/ic300366m | Inorg. Chem. 2012, 51, 6719−6730

fully optimized with the Turbomole program[40a] coupled to the PQS Baker optimizer[41] at the BP86 level,[42] using the def-TZVP basis.[40c,f] EPR parameters[43] were subsequently calculated with ORCA,[44] using the coordinates from the structure optimized in Turbomole as input. In the Orca calculations, we used the Ahlrich's def2-TZVP basis set, using both the B3LYP and the BP86 functional in separate calculations.[45] The B3LYP functional and a triple-ζ basis sets with one-set of polarization functions (TZV(P)) for all atoms were also employed for the population analyses and the calculation of the Mössbauer spectroscopic parameters,[46] which where also performed with ORCA. The "core" CP(PPP) basis set for iron with enhanced integration accuracy at iron was used for calculating the Mössbauer spectroscopic parameters.[47] Reduced orbital charges and orbital spin densities were calculated according to Löwdin population analysis.[48] Reduced orbital population is defined as a population per angular momentum type meaning the decomposition of the total spin or charge population at the given atom into the population of s, p_i, d_i, and f_i orbitals of the atom. Molecular orbitals and the spin density plots were visualized via the program Molekel.[49]

■ ASSOCIATED CONTENT

Supporting Information

Variable temperature ^{1}H NMR spectra of **K1** and **K2**; the results of the TD-DFT calculations, the cyclic voltammograms of complexes **1** and **2**, and Cartesian coordinates of the DFT-optimized structures, and X-ray crystallographic files in CIF format for **K2** and **2**. This material is available free of charge via the Internet at http://pubs.acs.org.

■ AUTHOR INFORMATION

Corresponding Author

*E-mail: robert.wolf@ur.de.

Notes

The authors declare no competing financial interest.

■ ACKNOWLEDGMENTS

Dedicated to Prof. Ulrich Zenneck (University of Erlangen-Nuremberg). We would like to thank Dipl.-Chem. K. Weber for conducting some preliminary experiments, Dr. J. J. Weigand for providing electrochemistry equipment and fruitful discussions, and Prof. W. Uhl (University of Münster) and Dr. E. Bill (MPI for Bioinorganic Chemistry, Mülheim) for support and advice. Funding from the Deutsche Forschungsgemeinschaft (WO1496/3-1 and 4-1), the Fonds der Chemischen Industrie (fellowships to R.W., M.M.K., and E.-M.S.) and The Netherlands Organization for Scientific Research (NWO middelgroot funding for EPR spectroscopy), is gratefully acknowledged. F.H. wants to acknowledge the University of Amsterdam (FNWI) for the construction and maintenance of the low-T OTTLE cells, and the University of Reading for financial support.

■ REFERENCES

(1) (a) Henrici-Olivé, G.; Olivé, S. *J. Am. Chem. Soc.* **1970**, *92*, 4831. (b) Elschenbroich, C.; Möckel, R. *Angew. Chem., Int. Ed. Engl.* **1977**, *16*, 870. (c) Datta, S.; Wreford, S. S. *Inorg. Chem.* **1977**, *16*, 1134.

(2) Ellis, J. E. *Inorg. Chem.* **2006**, *45*, 3167.

(3) Complexes with Ti, Zr, Hf, Nb, and Ta: (a) Jang, M.; Ellis, J. E. *Angew. Chem., Int. Ed. Engl.* **1994**, *33*, 1973. (b) Brennessel, W. W.; Ellis, J. E.; Roush, S. N.; Strandberg, B. R.; Woisetschläger, O. E.; Young, V. G., Jr. *Chem. Commun.* **2002**, 2356. (c) Brennessel, W. W.; Ellis, J. E.; Pomije, M. K.; Sussman, V. J.; Urnezius, E.; Young, V. G., Jr. *J. Am. Chem. Soc.* **2002**, *124*, 10258. (d) Brennessel, W. W.; Jilek, R. E.; Ellis, J. E. *Angew. Chem., Int. Ed.* **2007**, *46*, 6132. (e) Jilek, R. E.; Jang, M.; Smolensky, R. D.; Britton, J. D.; Ellis, J. E. *Angew. Chem., Int. Ed.* **2008**, *47*, 8692.

(4) Mn complexes: (a) Jonas, K.; Burkart, G.; Häselhoff, C.; Betz, P.; Krüger, C. *Angew. Chem., Int. Ed. Engl.* **1990**, *29*, 323. (b) Jonas, K.; Häselhoff, C.-C.; Goddard, R.; Krüger, C. *Inorg. Chim. Acta* **1992**, *198–200*, 533. (c) Thompson, R. L.; Lee, S.; L.; Rheingold, A.; Cooper, N. J. *Organometallics* **1991**, *10*, 1657.

(5) Fe complexes: Brennessel, W. W.; Jilek, R. E.; Ellis, J. E. *Angew. Chem., Int. Ed.* **2007**, *46*, 6132.

(6) Co complexes: (a) Brennessel, W. W.; Young, V. G., Jr.; Ellis, J. E. *Angew. Chem., Int. Ed.* **2002**, *41*, 1211. (b) Brennessel, W. W.; Young, V. G., Jr.; Ellis, J. E. *Angew. Chem., Int. Ed.* **2006**, *45*, 7268.

(7) Seaburg, J. K.; Fischer, P. J.; Young, V. G.; Ellis, J. E. *Angew. Chem., Int. Ed.* **1998**, *37*, 155.

(8) Ellis, J. E. *Organometallics* **2003**, *22*, 3322.

(9) (a) Barybin, M. V.; Young, V. G., Jr.; Ellis, J. E. *J. Am. Chem. Soc.* **1998**, *120*, 429. (b) Barybin, M. V.; Young, V. G., Jr.; Ellis, J. E. *J. Am. Chem. Soc.* **2000**, *122*, 4678. (c) Barybin, M. V.; Young, V. G., Jr.; Ellis, J. E. *J. Am. Chem. Soc.* **1999**, *121*, 9237. (d) Barybin, M. V.; Young, V. G., Jr.; Ellis, J. E. *Organometallics* **1999**, *18*, 2744. (e) Barybin, M. V.; Brennessel, W. W.; Kucera, B. E.; Minyaev, M. E.; Sussman, V. J.; Young, V. G., Jr.; Ellis, J. E. *J. Am. Chem. Soc.* **2007**, *129*, 1141. (f) Brennessel, W. W.; Ellis, J. E. *Angew. Chem., Int. Ed.* **2007**, *46*, 598.

(10) Urnėžius, E.; Brennessel, W. W.; Cramer, C. J.; Ellis, J. E.; Schleyer, P. v. R. *Science* **2002**, *295*, 832.

(11) (a) Wolf, R.; Ehlers, A. W.; Slootweg, J. C.; Lutz, M.; Gudat, D.; Hunger, M.; Spek, A. L.; Lammertsma, K. *Angew. Chem., Int. Ed.* **2008**, *47*, 4584. (b) Wolf, R.; Slootweg, J. C.; Ehlers, A. W.; Hartl, F.; de Bruin, B.; Lutz, M.; Spek, A. L.; Lammertsma, K. *Angew. Chem., Int. Ed.* **2009**, *48*, 3104. (c) Wolf, R.; Ehlers, A. W.; Khusniyarov, M. M.; Hartl, F.; de Bruin, B.; Long, G. J.; Grandjean, F.; Schappacher, M.; Pöttgen, R.; Slootweg, J. C.; Lutz, M.; Spek, A. L.; Lammertsma, K. *Chem.—Eur. J.* **2010**, *16*, 14322.

(12) Wolf, R.; Ghavtadze, N.; Weber, K.; Schnöckelborg, E.-M.; de Bruin, B.; Ehlers, A. W.; Lammertsma, K. *Dalton Trans.* **2010**, *39*, 1453.

(13) Weber, K.; Schnöckelborg, E.-M.; Wolf, R. *ChemCatChem* **2011**, *3*, 1572–1577.

(14) (a) Lacoste, M.; Astruc, D. *J. Chem. Soc., Chem. Commun.* **1987**, 667. (b) Lacoste, M.; Rabaa, H.; Astruc, D.; Le Beuze, A.; Saillard, J. Y.; Precigoux, G.; Courseille, C.; Ardoin, N.; Bowyer, W. *Organometallics* **1989**, *8*, 2233.

(15) Zhu, G.; Janak, K. E.; Figueroa, J. S.; Parkin, G. *J. Am. Chem. Soc.* **2006**, *128*, 5452.

(16) Preliminary communications: (a) Wolf, R.; Schnöckelborg, E.-M. *Chem. Commun.* **2010**, 2832. (b) Schnöckelborg, E.-M.; Weigand, J. J.; Wolf, R. *Angew. Chem., Int. Ed.* **2011**, *50*, 6657–6660.

(17) Related complexes: (a) Frings, A. Ph.D. Dissertation, Ruhr-Universität Bochum, Bochum, Germany, 1988. (b) Jonas, K. *Pure Appl. Chem.* **1990**, *62*, 1169–1174. (c) Klusmann, M. Ph.D. Dissertation, Ruhr-Universität Bochum, Bochum, Germany, 1993. (d) Brodt, C.; Niu, S.; Pritzkow, H.; Stephan, M.; Zenneck, U. *J. Organomet. Chem.* **1993**, *459*, 283. (e) Brodt, C.; Niu, S.; Pritzkow, H.; Stephan, M.; Zenneck, U. *J. Organomet. Chem.* **1993**, *459*, 283. (f) Kubo, H.; Hirano, M.; Komiya, S. *J. Organomet. Chem.* **1998**, *556*, 89.

(18) The nature of the species present in these mixtures of Cp*Li and $FeCl_2(thf)_{1.5}$ is not entirely clear, but we were able to crystallize and crystallographically characterize the salt $[Li(dme)_3][Cp^*FeCl_2]$. It seems likely that such ate-complexes are present in solution as well.

(19) Complex **2** could not be isolated from the 1:1 reaction of potassium anthracene and "Cp*FeCl", but the dinuclear complex $[Cp^*Fe(\mu\text{-}\eta^4\text{:}\eta^4\text{-}C_{14}H_{10})FeCp^*]$ (**2**) was obtained instead. Schnöckelborg, E.-M.; Hartl, F.; Langer, T.; Pöttgen, R.; Wolf, R. *Eur. J. Inorg. Chem.* **2012**, 1632–1638. For recent, related work see: Hatanaka, T.; Ohki, Y.; Kamachi, T.; Nakayama, T.; Yoshizawa, K.; Katada, M.; Tatsumi, K. *Chem.—Asian J.* DOI: 10.1002/asia.201101037.

(20) (a) Becke, A. D. *Phys. Rev. A* **1988**, *38*, 3098−3100. (b) Perdew, J. P. *Phys. Rev. B* **1986**, *34*, 7406. (c) Perdew, J. P. *Phys. Rev. B* **1986**, *33*, 8822.
(21) Sierka, M.; Hogekamp, A.; Ahlrichs, R. *J. Chem. Phys.* **2003**, *118*, 9136.
(22) (a) Ahlrichs, R.; Bär, M.; Häser, M.; Horn, H.; Kölmel, C. *Chem. Phys. Lett.* **1989**, *162*, 165. (b) Treutler, O.; Ahlrichs, R. *J. Chem. Phys.* **1995**, *102*, 346.
(23) The cation $\mathbf{1}^+$ has previously been synthesized and spectroscopically characterized in the salt $[Cp^*Fe(\eta^6\text{-}C_{10}H_8)]PF_6$ (**1PF$_6$**), but its X-ray structure was not determined. Its cyclic voltammogram shows two reversible reduction steps in DMF at −1.73 and −2.29 V vs Fc/Fc^+.[14]
(24) Temperature-dependent NMR behavior has previously been observed for the titanium complexes $[Cp^*Ti(\eta^4\text{-}C_{14}H_{10}(\eta^2\text{-}C_{14}H_{10})]^{2-}$, $[Ti(\eta^4\text{-}C_{10}H_8)_3]^{2-}$, and $[Ti(\eta^4\text{-}C_{14}H_{10})_3]$.[2,3e,7]
(25) (a) Rieke, R. D.; Henry, W. P.; Arney, I. S. *Inorg. Chem.* **1987**, *26*, 420. (b) Schäufele, H.; Hu, D.; Pritzkow, H.; Zenneck, U. *Organometallics* **1989**, *8*, 396. (c) Jonas, K.; Häsellhoff, C.-C.; Goddard, R.; Krüger, C. *Inorg. Chim. Acta* **1987**, *198*, 533. (d) Brodt, C.; Niu, S.; Pritzkow, H.; Stephan, M.; Zenneck, U. *J. Organomet. Chem.* **1993**, *459*, 283.
(26) CV measurements of **1** in THF/Bu_4NPF_6 at variable scan rates between v = 0.05−1.00 V s^{-1} showed a decrease of the anodic counterpeak of the reduction $\mathbf{1}\rightarrow\mathbf{1}^-$ with scan rates lower than 0.2 V s^{-1}. We attribute this observation to the slow decomposition of $\mathbf{1}^-$ because of its reaction with the electrolyte Bu_4NPF_6. Cf. the Supporting Information, Figure S15 for further details.
(27) Conelly, N. G.; Geiger, W. E. *Chem. Rev.* **1996**, *96*, 877−910.
(28) (a) Khusniyarov, M. M.; Bill, E.; Weyhermüller, T.; Bothe, E.; Harms, K.; Sundermeyer, J.; Wieghardt, K. *Chem.—Eur. J.* **2008**, *14*, 7608−7622. (b) Khusniyarov, M. M.; Weyhermüller, T.; Bill, E.; Wieghardt, K. *J. Am. Chem. Soc.* **2009**, *131*, 1208.
(29) (a) Nesmeyanov, A. N.; Vol'kenau, N. A.; Bolesova, I. N. *Dokl. Akad. Nauk SSSR* **1966**, *166*, 607. (b) Nesmeyanov, A. N.; Vol'kenau, N. A.; Shilovtseva, L. S. *Izv. Akad. Nauk SSSR, Ser. Khim.* **1970**, 1206. (c) Sutherland, R. G.; Chen, S. C.; Pannekoek, J.; Lee, C. C. *J. Organomet. Chem.* **1975**, *101*, 221. (d) Sutherland, R. G.; Chen, S. C.; Pannekoek, W. J.; Lee, C. C. *J. Organomet. Chem.* **1976**, *117*, 61. (e) Azogu, C. I. *Anal. Chim. Acta* **1981**, *125*, 171. (f) Desobry, V.; Kündig, E. P. *Helv. Chim. Acta* **1981**, *64*, 1288. (g) Schumann, H. *Chem.-Ztg.* **1982**, *106*, 369. (h) Guerchais, V.; Astruc, D. *J. Chem. Soc., Chem. Commun.* **1983**, 1115. (i) Guerchais, V.; Astruc, D. *J. Organomet. Chem.* **1986**, *312*, 97. (j) Kubicki, M. M.; Gautheron, B.; Steinfeldt, W.; Singer, H. *Inorg. Chim. Acta* **1992**, *192*, 211. (k) Kündig, E. P.; Jeger, P.; Bernardinelli, G. *Angew. Chem., Int. Ed. Engl.* **1995**, *34*, 2161. (l) Decken, A.; Rigby, S. S.; Girard, L.; Bain, A. D.; McGlinchey, M. J. *Organometallics* **1997**, *16*, 1308. (m) Masterson, D. S.; Tratz, C. M.; Behrens, B. A.; Glatzhofer, D. T. *Organometallics* **2000**, *19*, 244. (n) Kündig, E. P.; Jeger, P.; Bernardinelli, G. *Inorg. Chim. Acta* **2004**, *357*, 1909. (o) Reingold, J. A.; Virkaitis, K. L.; Carpenter, G. B.; Sun, S.; Sweigart, D. A.; Czech, P. T.; Overly, K. R. *J. Am. Chem. Soc.* **2005**, *127*, 11146. (p) Amaya, T.; Sakane, H.; Hirao, T. *Angew. Chem., Int. Ed.* **2007**, *46*, 8376. (q) Sakane, H.; Amaya, T.; Moriuchi, T.; Hirao, T. *Angew. Chem., Int. Ed.* **2009**, *48*, 1640. (r) Zanello, P.; Fedi, S.; Fabrizi, d. B. F.; Giorgi, G.; Amaya, T.; Sakane, H.; Hirao, T. *Dalton Trans.* **2009**, 9192.
(30) (a) Nesmeyanov, A. N.; Denisovich, L. I.; Gubin, S. P.; Vol'kenau, N. A.; Sirotkina, E. I.; Bolesova, I. N. *J. Organomet. Chem.* **1969**, *20*, 169. (b) Nesmeyanov, A. N.; Vol'kenau, N. A.; Shilovtseva, L. S.; Petrakova, V. A. *J. Organomet. Chem.* **1973**, *61*, 329. (c) Nesmeyanov, A. N.; Sinitsyna, N. A.; Kotova, L. S.; Kolesov, V. S.; Sizoi, V. F.; Vol'kenau, N. A. *Dokl. Akad. Nauk SSSR* **1978**, *242*, 1356. (d) Nesmeyanov, A. N.; Solodovnikov, S. P.; Vol'kenau, N. A.; Kotova, L. S.; Sinitsyna, N. A. *J. Organomet. Chem.* **1978**, *148*, C5.
(31) (a) Goodman, B. A.; Raynor, J. B. Electron Spin Resonance of Transition Metal Complexes. In *Advances in Inorganic Chemistry and Radiochemistry*; H. J. Emeléus, Sharpe, A. G., Eds.; Academic Press: New York, 1970; Vol. *13*, p 136. (b) Hetterscheid, D. G. H.; Grützmacher, H.; Koekoek, A. J. J.; de Bruin, B. *Prog. Inorg. Chem.* **2007**, *55*, 247.
(32) (a) Vlcek, A. A. *Z. Anorg. Allg. Chem.* **1960**, *304*, 109. (b) Vlcek, A. A. *Collect. Czech. Chem. Commun.* **1965**, *30*, 952.
(33) Parish, R. V. *The Organic Chemistry of Iron*; Academic Press: New York, 1978; Vol. *1*, Mössbauer Spectroscopy, p 176.
(34) (a) Jutzi, P.; Schwartzen, K.-H.; Mix, A. *Chem. Ber.* **1990**, *123*, 837. (b) Jonas, K.; Klusmann, P.; Goddard, R. *Z. Naturforsch. B* **1995**, *50*, 394.
(35) Haberditzl, W. *Angew. Chem.* **1966**, *78*, 277.
(36) (a) *SHELXTL-Plus*, REL. 4.1; Siemens Analytical X-ray Instruments Inc.: Madison, WI, 1990. (b) Sheldrick, G. M. *SHELXL 97*, Program for the Refinement of Structures; University of Göttingen: Göttingen, Germany, 1997.
(37) Mahabiersing, T.; Luyten, H.; Nieuwendam, R. C.; Hartl, F. *Collect. Czech. Chem. Commun.* **2003**, *68*, 1687−1709.
(38) Brand, R. A. *NORMOS-90 Mössbauer Fitting Program*; University of Duisburg: Essen, Germany, 2002.
(39) (a) Weigend, F.; Ahlrichs, R. *Phys. Chem. Chem. Phys.* **2005**, *7*, 3297. (b) Andrae, D.; Häussermann, U.; Dolg, M.; Stoll, H.; Preuss, H. *Theor. Chim. Acta* **1990**, *77*, 123−141.
(40) (a) Ahlrichs, R.; Bär, M.; Baron, H.-P.; Bauernschmitt, R.; Böcker, S.; Ehrig, M.; Eichkorn, K.; Elliott, S.; Furche, F.; Haase, F.; Häser, M.; Hättig, C.; Horn, H.; Huber, C.; Huniar, U.; Kattannek, M.; Köhn, A.; Kölmel, C.; Kollwitz, M.; May, K.; Ochsenfeld, C.; Öhm, H.; Schäfer, A.; Schneider, U.; Treutler, O.; Tsereteli, K.; Unterreiner, B.; von Arnim, M.; Weigend, F.; Weis, P.; Weiss, H. *Turbomole Version 5*; Theoretical Chemistry Group, University of Karlsruhe: Karlsruhe, Germany, 2002; (b) Treutler, O.; Ahlrichs, R. *J. Chem. Phys.* **1995**, *102*, 346. (c) Turbomole basis set library, Turbomole Version 5, see ref 40a. (d) Schäfer, A.; Horn, H.; Ahlrichs, R. *J. Chem. Phys.* **1992**, *97*, 2571. (e) Andrae, D.; Häussermann, U.; Dolg, M.; Stoll, H.; Preuss, H. *Theor. Chim. Acta* **1990**, *77*, 123. (f) Schäfer, A.; Huber, C.; Ahlrichs, R. *J. Chem. Phys.* **1994**, *100*, 5829.
(41) (a) *PQS*, version 2.4; Parallel Quantum Solutions: Fayetteville, AK, 2001; (the Baker optimizer is available separately from PQS upon request). (b) Baker, J. *J. Comput. Chem.* **1986**, *7*, 385.
(42) (a) Lee, C.; Yang, W.; Parr, R. G. *Phys. Rev. B* **1988**, *37*, 785. (b) Becke, A. D. *J. Chem. Phys.* **1993**, *98*, 1372. (c) Becke, A. D. *J. Chem. Phys.* **1993**, *98*, 5648.
(43) Some references and reviews on DFT approaches to EPR parameters: (a) van Lenthe, E.; van der Avoird, A.; Wormer, P. E. S. *J. Chem. Phys.* **1997**, *107*, 2488. (b) van Lenthe, E.; van der Avoird, A.; Wormer, P. E. S. *J. Chem. Phys.* **1998**, *108*, 4783. (c) Neese, F. *Curr. Opin. Chem. Biol.* **2003**, *7*, 125. (d) Neese, F.; Solomon, E. In *Magnetoscience- From Molecules to Materials*; Miller, J. S., Drillon, M., Eds.; Wiley: New York, 2003; p 345. (e) Peng, G.; Nichols, J.; McCullough, E. A.; Spence, J. *Inorg. Chem.* **1994**, *33*, 2857.
(44) Neese, F. *ORCA, An ab initio, Density Functional and Semiempirical program package*, versions 2.7.0 and 2.8.0; University of Bonn: Bonn, Germany, 2009.
(45) (a) Lee, C.; Yang, W.; Parr, R. G. *Phys. Rev. B* **1988**, *37*, 785. (b) Becke, A. D. *J. Chem. Phys.* **1993**, *98*, 1372. (c) Becke, A. D. *J. Chem. Phys.* **1993**, *98*, 5648.
(46) Schäfer, A.; Horn, H.; Ahlrichs, R. *J. Chem. Phys.* **1992**, *97*, 2571.
(47) (a) Neese, F. *Inorg. Chim. Acta* **2002**, *337*, 181. (b) Sinnecker, S.; Slep, L. D.; Bill, E.; Neese, F. *Inorg. Chem.* **2005**, *44*, 2245.
(48) (a) *ORCA manual*, version 2.6-35; February 2007; p 296. (b) Löwdin, P. O. *J. Chem. Phys.* **1950**, *18*, 365−375. (c) Löwdin, P. O. *Adv. Quantum Chem.* **1970**, *5*, 185.
(49) Portmann, S. *Molekel*, version 4.3.win32; CSCS/University of Geneva: Geneva, Switzerland, 2002.